Bifurcation analysis of eight coupled degenerate optical parametric oscillators

Daisuke Ito[a,b,*], Tetsushi Ueta[c], Kazuyuki Aihara[d]

[a] *Department of Electronic Systems Engineering, University of Shiga Prefecture, 2500 Hassaka-cho Hikone, Shiga, 522-8533, Japan*
[b] *Department of Electrical, Electronic and Computer Engineering, Gifu University, 1-1 Yanagido Gifu, Gifu, 501-1193, Japan*
[c] *Center for Administration of Information Technology, Tokushima University, 2-1 Minami-Josanjima Tokushima, Tokushima, 770-8506, Japan*
[d] *Institute of Industrial Science, University of Tokyo, 4-6-1 Komaba Meguro-ku, Tokyo, 152-8505, Japan*

Abstract

A degenerate optical parametric oscillator (DOPO) network realized as a coherent Ising machine can be used to solve combinatorial optimization problems. Both theoretical and experimental investigations into the performance of DOPO networks have been presented previously. However a problem remains, namely that the dynamics of the DOPO network itself can lower the search success rates of globally optimal solutions for Ising problems. This paper shows that the problem is caused by pitchfork bifurcations due to the symmetry structure of coupled DOPOs. Some two-parameter bifurcation diagrams of equilibrium points express the performance deterioration. It is shown that the emergence of non-ground states regarding local minima hampers the system from reaching the ground states corresponding to the global minimum. We then describe a parametric strategy for leading a system to the ground state by actively utilizing the bifurcation phenomena. By adjusting the parameters to break particular symmetry, we find appropriate parameter sets that allow the coherent Ising machine to obtain the globally optimal solution alone.

Keywords: bifurcation analysis, degenerate optical parametric oscillators, symmetry-breaking bifurcations

---

[*]Corresponding author
  Email addresses: `d_ito@gifu-u.ac.jp` (Daisuke Ito), `ueta@tokushima-u.ac.jp` (Tetsushi Ueta), `aihara@sat.t.u-tokyo.ac.jp` (Kazuyuki Aihara)

1. Introduction

Recently, Yamamoto et al. have developed a practical coherent Ising machine (CIM) by utilizing the criticality of an injection-locked laser [1, 2, 3] to find good approximate solutions of NP-hard problems [4]. A CIM can solve these problems by using the binary phase of an optical oscillator to represent the Ising spin. Such a machine has already been realized by applying a laser network that consists of degenerate optical parametric oscillators (DOPOs) and a measurement-feedback field-programmable gate array circuit, and its performance has been evaluated in laboratory experiments [2, 5, 6, 7]. It has been confirmed that a lot of trials found the global-optimal solutions, but some trials got stuck at local optima. Therefore, the probability of finding the global-optimal solutions is less than 100% [5, 6, 7, 8].

Wang et al. presented a mathematical model of a CIM based on c-number Langevin equations [8, 9]. Stability analysis of the two-coupled model proves that a bifurcation produces the correct solutions to the Ising problem of two spins with antiferromagnetic coupling. On the other hand, the MAX-CUT problem, which is the problem of finding a maximum cut in a given graph, is a well-known NP-hard problem [10] that has various applications in addition to its theoretical importance [11]. By taking Ising models in the form of non-directional and unweighted graphs, a CIM can solve the MAX-CUT problem under appropriate circumstances. The validity of a CIM as a MAX-CUT problem solver has been examined both experimentally and numerically [6, 7, 12]; the results provide empirical evidence of good approximation performance that is equivalent to or better than that of simulated annealing but requiring much less computation time. These results show that the CIMs are aptly applicable to high-speed computation for various combinatorial optimization problems. However, CIM performance can be disrupted by local-optimal solutions that might be due to not only the machine scheme but also to its dynamical properties.

A study of a cubic graph with eight vertices confirmed that steady states corresponding to local-optimal solutions were produced by bifurcation phenomena near but less than the oscillation threshold of a DOPO [9]. With further increase of its pump rate, the ground state corresponding to the global-optimal solution emerged. Ideally, we ex-

pect that a CIM converges to ground states corresponding to global optima. However, many local-optimal points appear via various bifurcation phenomena caused by increasing the pump rate, and the global-optimal points co-exist with these local-optimal ones in the state space. In general, we cannot expect a large domain of attraction to be associated with the global-optimal points. Therefore, it is difficult to specify initial values from which the CIM can find steady states corresponding to global-optimal points. Thus, the probability of success drops below unity. The aforementioned dynamical behavior should be related to the bifurcation phenomena and multi-stability that are typically observed in nonlinear dynamical systems [13], thus a thorough investigation of bifurcations in CIMs may give a clue why this performance deterioration occurs.

In the present paper, we analyze bifurcation phenomena in DOPO networks. We begin by describing a particular symmetry property of a transformation-invariant DOPO model. Next, we focus on the bifurcation structures of single and coupled DOPOs with various pump rates. By visualizing bifurcation structures, we clarify the critical pump rate and its relationship with CIM performance. Finally, we discuss a new control strategy to improve CIM performance.

2. Mathematical model of DOPOs

A DOPO with a measurement and feedback scheme is described by the following c-number Langevin equations [6, 7]:

$$
\begin{aligned}
dc &= \left(-1 + p - c^2 - s^2\right) c\, dt + \frac{1}{A_s} \sqrt{c^2 + s^2 + \frac{1}{2}}\, dW_1, \\
ds &= \left(-1 - p - c^2 - s^2\right) s\, dt + \frac{1}{A_s} \sqrt{c^2 + s^2 + \frac{1}{2}}\, dW_2,
\end{aligned}
\tag{1}
$$

where c and s are the normalized in-phase and quadrature-phase components, respectively, p is the pump rate, -1 and $p - (c^2 + s^2)$ are the loss and saturated gain, respectively, A_s is the saturation amplitude, and W_1 and W_2 are independent standard Brownian motions. The differential equations without Brownian motions for an $N \times N$

3

sized network of DOPOs are expressed as follows [8, 9]:

$$\frac{d}{dt}c_j = f(c_j,\ s_j) + \sum_{l=1,\ l \neq j}^{N} \xi_{jl} c_l = \left(-1 + p - (c_j^2 + s_j^2)\right) c_j + \sum_{l=1,\ l \neq j}^{N} \xi_{jl} c_l,$$

$$\frac{d}{dt}s_j = g(c_j,\ s_j) + \sum_{l=1,\ l \neq j}^{N} \xi_{jl} s_l = \left(-1 - p - (c_j^2 + s_j^2)\right) s_j + \sum_{l=1,\ l \neq j}^{N} \xi_{jl} s_l,$$

$$(2)$$

where ξ_{jl} is the coupling coefficient between nodes j and l. A detailed description of the quantum models is shown in Refs. [14, 15].

If we define the state vectors $\boldsymbol{c} = (c_1,\ c_2,\ \ldots,\ c_N)^\top$ and $\boldsymbol{s} = (s_1,\ s_2,\ \ldots,\ s_N)^\top$, then

$$\frac{d}{dt}\boldsymbol{c} = \boldsymbol{f}(\boldsymbol{c},\ \boldsymbol{s}) + \Xi\boldsymbol{c},$$

$$\frac{d}{dt}\boldsymbol{s} = \boldsymbol{g}(\boldsymbol{c},\ \boldsymbol{s}) + \Xi\boldsymbol{s},$$

$$(3)$$

where

$$\boldsymbol{f}(\boldsymbol{c},\ \boldsymbol{s}) = (f(c_1,\ s_1),\ f(c_2,\ s_2),\ \ldots,\ f(c_N,\ s_N))^\top,$$

$$\boldsymbol{g}(\boldsymbol{c},\ \boldsymbol{s}) = (g(c_1,\ s_1),\ g(c_2,\ s_2),\ \ldots,\ g(c_N,\ s_N))^\top.$$

$$(4)$$

We assume that the coupling coefficients are represented as a symmetric matrix Ξ as follows (i.e., all connections are non-directional and mutual):

$$\Xi = \begin{pmatrix} 0 & \xi_{12} & \cdots & \xi_{1N} \\ \xi_{21} & 0 & & \xi_{2N} \\ \vdots & & \ddots & \\ \xi_{N1} & \xi_{N2} & & 0 \end{pmatrix}, \quad \text{where} \quad \xi_{jl} = \xi_{lj}, \quad j = 1,\ 2,\ \ldots,\ N. \quad (5)$$

Let us consider the formulation of the Ising problem [16] from the DOPO model given by Eq. (2). The Ising Hamiltonian is given as

$$H = -\sum_{1 \leq j < l \leq N} \xi_{jl} x_j x_l, \tag{6}$$

where x_j is the Ising spin and ξ_{jl} is the interaction coefficient between nodes j and l. We omit the Zeeman term for simplicity. The DOPO has a bistable oscillatory phase corresponding to the spin mode $x_j = \pm 1$ in the Ising Hamiltonian. If we define the spin state $\boldsymbol{x} = (x_1,\ x_2, \ldots,\ x_N)^\top$, then

$$x_j = \frac{c_j}{|c_j|}. \tag{7}$$

4

From the above definitions, any node can be classified based on the sign of c_j in the steady state.

The Ising problem includes the MAX-CUT problem of determining the maximum cut size in a graph [17]. The Ising Hamiltonian can be mapped to the cut size in the MAX-CUT problem, thus the ground states of the Ising Hamiltonian correspond to the maximum cut size. In general, these problems are known to be NP-complete. We define the cut size cut(Ξ, x) as follows:

$$\text{cut}(\Xi, x) = -\sum_{j=1}^{N} \sum_{l=1, l \neq j}^{N} J_{jl} x_j x_l, \quad x \in \{+1, -1\}, \tag{8}$$

where $x = (x_1, x_2, \ldots, x_j)^\top \in \{-1, +1\}^N$ represents the grouping expressed by cutting. The term J_{jl} is the generic element of the coupling matrix and is defined as $J_{jl} = 0$ if $\xi_{jl} = 0$ or $J_{jl} = 1$ otherwise.

Equation (2) with negative coupling strength basically tends to keep the ground state as the stable equilibrium point. When the DOPO network is in the ground state, the relaxation function $\eta(c)$ shown in Eq. (9) takes the smallest value.

$$\eta(c) = \sum_{j=1}^{N} (p - c_j^2 - 1) = -\sum_{j=1}^{N} \sum_{l=1, l \neq j}^{N} \xi_{jl} \frac{c_l}{c_j}. \tag{9}$$

2.1. Symmetry of DOPO model

Let us consider a particular symmetry property of the DOPO model. An autonomous system is written in the form $dx/dt = f(x)$, where $f : R^n \rightarrow R^n$ is a C^∞-class function for $x \in R^n$. Assume that we have a transformation P such that

$$\begin{aligned} P : \quad & R^n \rightarrow R^n, \\ & x \mapsto Px. \end{aligned} \tag{10}$$

If the system satisfies

$$f(Px) = Pf(x) \quad \forall x \in R^n \tag{11}$$

then it is called P-invariant [18, 19].

First, we consider the single model as follows:

$$\frac{d}{dt} z = f(z, p) = \begin{pmatrix} \left(-1 + p - (c_1^2 + s_1^2)\right) c_1 \\ \left(-1 - p - (c_1^2 + s_1^2)\right) s_1 \end{pmatrix}, \tag{12}$$

5

where $z = (c_1, s_1)^\top$ is a state vector. Now I_n is an $n \times n$ identity matrix. If we define the transformation $P_1 = -I_2$, then

$$f(P_1 z, p) = f(-z, p) = \begin{pmatrix} -\left(-1 + p - (c_1^2 + s_1^2)\right) c_1 \\ -\left(-1 - p - (c_1^2 + s_1^2)\right) s_1 \end{pmatrix} = P_1 f(z, p), \qquad (13)$$

and thus

$$f(P_1 z, p) = P_1 f(z, p) \quad \forall c \in R^2. \qquad (14)$$

As a result, $P_1 = I_2$ and $P_1 = -I_2$ are P-invariant for Eq. (12). In other words, there exists a symmetry group Γ such that

$$\Gamma = \{I_2, -I_2\}. \qquad (15)$$

For $-I_2$ we have the following invariant transformation:

$$(c_1, s_1) \mapsto (-c_1, -s_1). \qquad (16)$$

Next, let us consider the DOPO network comprising N nodes. The state space is defined as $z = (c, s)^\top \in R^{2N}$. Equation (2) is also represented as follows:

$$\frac{d}{dt} z = F(z, p) + \Xi z, \qquad (17)$$

where $F : R^{2N} \to R^{2N}$ is a C^∞-class function that is defined as

$$F(z, p) = \begin{pmatrix} f(c, s, p) + \Xi c \\ g(c, s, p) + \Xi s \end{pmatrix}. \qquad (18)$$

If we define the transformation $P_N = -I_{2N}$, then

$$F(P_N z, p) = \begin{pmatrix} f(-c, -s, p) - \Xi c \\ g(-c, -s, p) - \Xi s \end{pmatrix}. \qquad (19)$$

From the above results that $f(-c, -s, p) = -f(c, s, p)$ and $g(-c, -s, p) = -g(c, s, p)$, clearly we have

$$F(P_N z, p) = P_N F(z, p). \qquad (20)$$

Consequently, $P_N = I_{2N}$ and $P_N = -I_{2N}$ are P-invariant for any network topology of Eq. (2). In other words, for $-I_{2N}$ we have the following invariant transformation:

$$(c, s) \mapsto (-c, -s). \qquad (21)$$

6

This symmetry property affects the dynamical behavior directly; for instance, equilibria may undergo pitchfork bifurcations [20]. For this symmetrical case, the bifurcations of equilibria can be classified by group theory [21].

2.2. Bifurcations of a single DOPO

First, we investigate the single c-number Langevin equation as given by Eq. (12). In this equation, at most three equilibrium points are possible: $C_0 = (0, 0)$, $C^+ = (\sqrt{p-1}, 0)$, and $C^- = (-\sqrt{p-1}, 0)$. From Eq. (12), the Jacobian matrix is given by

$$
Df(c_1) = \begin{bmatrix} -1 + p - 3c_1^2 - s_1^2 & -2c_1 s_1 \\ -2c_1 s_1 & -1 - p - c_1^2 - 3s_1^2 \end{bmatrix},
\tag{22}
$$

where $c_1 = (c_1, s_1)^\top \in \mathbf{R}^2$. By substituting the equilibrium points into Eq. (22), we obtain the characteristic equations of these equilibrium points and subsequently their eigenvalues:

$$
\mu(C_0) = -1 \pm p, \quad \mu(C^\pm) = 2 - 2p, -2p.
\tag{23}
$$

Thus, C_0 is a stable equilibrium point at any $p < 1$, but becomes unstable at $p = 1$ through a supercritical pitchfork bifurcation. Thereupon, two equilibrium points $C^\pm$ appear that are stable for any $p > 1$. The relationship between the parameter p and the stability of the equilibrium points is given in Table 1.

Table 1: Equilibria and their stabilities for a single DOPO.

$p < 1$	C_0: stable node
$p = 1$	supercritical pitchfork bifurcation of C_0
$p > 1$	C_0: saddle
	C^+, C^-: stable nodes

2.3. Numerical bifurcation analysis of a DOPO network

When considering a network of DOPOs, detailed analysis of all equilibrium points is not realistic because the dimension of the mathematical model of the network will be too high. For example, in an n-node network, there are $2^n + 1$ equilibrium points theoretically, namely 2^n combinatorial patterns and the origin. Accordingly, we rely on a heuristic algorithm to find the locations of the equilibrium points.

Now, let us consider an n-dimensional continuous-time dynamical system as $dc/dt = f(c, \lambda)$, where $c \in \mathbf{R}^n$ and $\lambda \in \mathbf{R}$. If c_0 is an equilibrium point, then the following condition is satisfied:

$$f(c_0, \lambda) = 0. \tag{24}$$

The stability of c_0 is given by the Jacobian matrix $\partial f / \partial c$. If the eigenvalues of the Jacobian matrix become zero or purely imaginary, the stability of c_0 changes; therefore, equilibrium points can undergo bifurcations. The characteristic equation of the equilibria is formulated as follows:

$$\chi(\mu) = \det\left(\frac{\partial f}{\partial c_0} - \mu I_n\right) = 0, \tag{25}$$

where the eigenvalue μ determines the target bifurcation type: $\mu = 0$ for a saddle-node or a pitchfork bifurcation and $\mu = e^{-ir}$ for a Hopf bifurcation, where i is the imaginary unit. The location of the equilibrium point c_0 and the bifurcation parameter value λ are obtained simultaneously for a given eigenvalue μ by solving the following equations for c and λ:

$$\Phi = \begin{pmatrix} f(c, \lambda) \\ \chi(\mu) \end{pmatrix} = 0. \tag{26}$$

This problem can be solved by using Newton's method. Some efficient computational schemes for Eq. (26) with relevant variational equations are given in [22, 23, 24, 25].

In the present study, we set $N = 8$ and assume that any node connects to three other nodes [8, 9]. The network topology is illustrated in Fig. 1, where the node numerals correspond to the index numbers of the state variables c and s. From Fig. 1, the coupling matrix Ξ is

$$\Xi = \begin{pmatrix} 0 & \xi & \xi & \xi & 0 & 0 & 0 & 0 \\ \xi & 0 & \xi & 0 & \xi & 0 & 0 & 0 \\ \xi & \xi & 0 & 0 & 0 & \xi & 0 & 0 \\ \xi & 0 & 0 & 0 & 0 & 0 & \xi & \xi \\ 0 & \xi & 0 & 0 & 0 & 0 & \xi & \xi \\ 0 & 0 & \xi & 0 & 0 & 0 & \xi & \xi \\ 0 & 0 & 0 & \xi & \xi & \xi & 0 & 0 \\ 0 & 0 & 0 & \xi & \xi & \xi & 0 & 0 \end{pmatrix}, \tag{27}$$

8

where we assume a uniform coupling strength ξ common to all edges. Note that each node tends to take the same sign ($x_j x_l > 0 \; \forall \; \xi_{jl} = \xi$) when $\xi > 0$, whereas each node tends to take the opposite sign to that of its connected nodes when $\xi < 0$. This topology admits the following two symmetrical transformations:

$$(c_1, c_2, c_3, c_4, c_5, c_6, c_7, c_8, s_1, s_2, s_3, s_4, s_5, s_6, s_7, s_8) \mapsto$$
$$\delta_1(\boldsymbol{c}, \boldsymbol{s}) = (c_2, c_3, c_1, c_5, c_6, c_4, c_7, c_8, s_2, s_3, s_1, s_5, s_6, s_4, s_7, s_8), \tag{28}$$

$$(c_1, c_2, c_3, c_4, c_5, c_6, c_7, c_8, s_1, s_2, s_3, s_4, s_5, s_6, s_7, s_8) \mapsto$$
$$\delta_2(\boldsymbol{c}, \boldsymbol{s}) = (c_1, c_2, c_3, c_4, c_5, c_6, c_8, c_7, s_1, s_2, s_3, s_4, s_5, s_6, s_8, s_7), \tag{29}$$

where δ_1 and δ_2 are the transformation matrixes expressing the maps given in Eqs. (28) and (29), respectively. Hence, we have the symmetry group

$$\Gamma = \{I_{16}, -I_{16}, \delta_1, \delta_2\}. \tag{30}$$
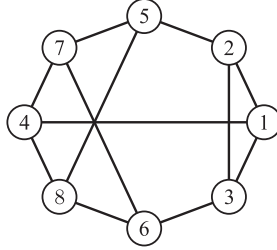
Figure 1: Network diagram. Each circle and edge correspond to a DOPO and a mutual connection, respectively.

In this network, the global-optimal and suboptimal solutions, namely the steady states with the highest and second-highest cut size given in Eq. (8) for the MAX-CUT problem, are listed in Table 2. These results were found by an exhaustive search.

Table 2: Cuts with the highest and second-highest cut size for the network in Fig. 1. Each symbol for x_j corresponds to the sign of c_j. In the network with eight nodes, there are $2^8 = 256$ solution patterns including overlapping.

	Optimal solutions								
No.	$(x_1$	x_2	x_3	x_4	x_5	x_6	x_7	$x_8)$	Cut size
i	−	−	+	+	+	+	−	−	16
ii	−	+	−	+	+	+	−	−	16
iii	−	+	+	−	−	−	+	+	16
iv	+	−	−	+	+	+	−	−	16
v	+	−	+	−	−	−	+	+	16
vi	+	+	−	−	−	−	+	+	16
	Suboptimal solutions								
No.	$(x_1$	x_2	x_3	x_4	x_5	x_6	x_7	$x_8)$	Cut size
vii	−	−	−	+	+	+	−	−	12
viii	−	−	+	−	−	−	+	+	12
ix	−	−	+	+	+	−	−	−	12
x	−	+	−	−	−	−	+	+	12
xi	−	+	−	+	−	+	−	−	12
xii	−	+	+	+	−	−	+	+	12
xiii	−	+	+	+	+	+	−	−	12
xiv	+	−	−	−	−	−	+	+	12
xv	+	−	−	−	+	+	−	−	12
xvi	+	−	+	−	+	−	+	+	12
xvii	+	−	+	+	+	+	−	−	12
xviii	+	+	−	−	−	+	+	+	12
xix	+	+	−	+	+	+	−	−	12
xx	+	+	+	−	−	−	+	+	12

3. Bifurcation structure of network with common pump rates

Next, we study the parametric dependency of the coupled c-number Langevin equations in Eq. (2) by exploring bifurcation diagrams of the equilibrium points. In the present study, we assume that the performance of the CIM is influenced mainly by bifurcations of stable equilibria, and we describe the relationship between these bifurcation structures and the CIM performance.

Figure 2 shows the bifurcation diagram in the p-ξ plane, where the symbols pf and G specify pitchfork and saddle-node bifurcations, respectively. The dashed lines are bifurcation parameter sets for unstable equilibrium points. Each bifurcation set is linear, and they are concentrated in $(p, \xi) = (1, 0)$, which corresponds to the pitchfork bifurcation of the single model. In region (i), there is the trivial equilibrium point at the origin; this becomes unstable and pairs of equilibrium points emerge around it through a supercritical pitchfork bifurcation. This scenario is caused by the state-space symmetry shown in Section 2.1 [19, 26]. Next, twelve unstable equilibrium points appear through two pitchfork bifurcations marked as pf+pf.
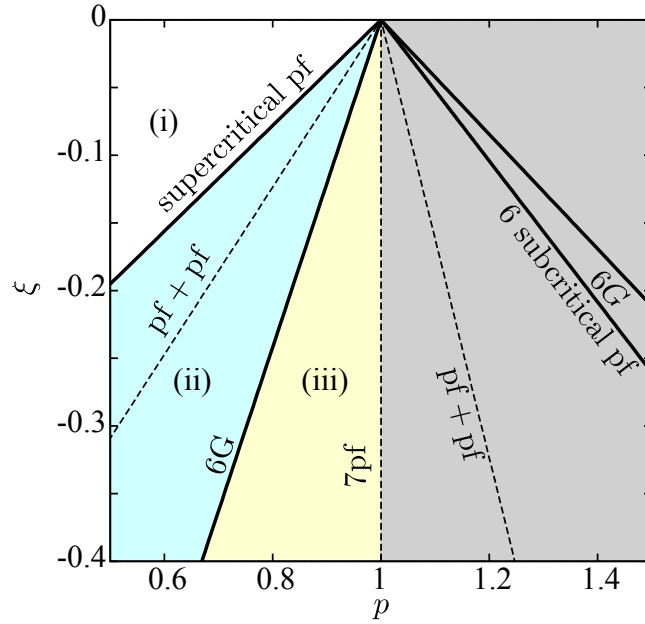
Figure 2: Bifurcation diagram in the p-ξ plane (pf=pitchfork bifurcation; G=saddle-node bifurcation). The dashed lines are bifurcation sets of unstable equilibrium points.
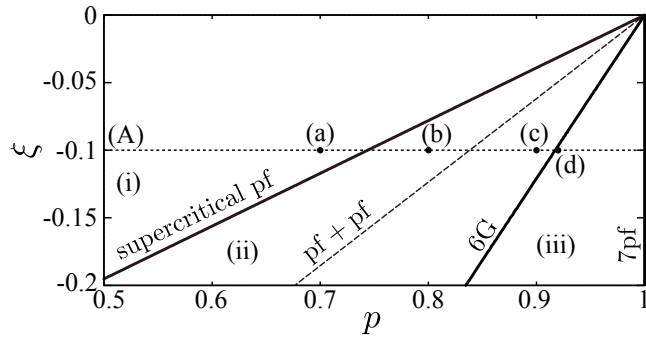
Figure 3: Enlarged part of Fig. 2.
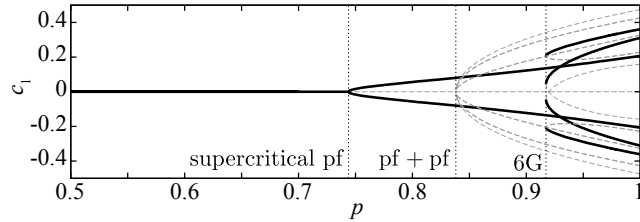
Figure 4: One-dimensional bifurcation diagram with $\xi = -0.1$. Solid and dashed lines represent stable and unstable equilibrium points, respectively.

Figure 3 shows an enlarged region of Fig. 2. Along the dashed line (A), the number of equilibrium points changes as p increases. Figure 4 shows a one-dimensional bifurcation diagram on line (A) in Fig. 3. This shows that stable equilibrium points appear via the pitchfork and six saddle-node bifurcations. Figure 5 shows the locations of equilibrium points in the c_1-c_2 plane for the points (a)–(d) in Fig. 3. Here, $_jO$ denotes an equilibrium point and j indicates the number of unstable eigenvalues. At $p = 0.7$, the trivial equilibrium point exists at the origin. As p is increased, many equilibrium points emerge around the origin by bifurcations.

With further increase of p, it is hard to compute the equilibria analytically. Figure 6 shows the stable equilibrium points for various values of p as computed numerically. We used a pseudo-random number generator [27] to create 50,000 initial points from which to seek equilibria by Newton's method. At $p = 1.8$, we found the 256 stable equilibrium points that represent all possible solution patterns in a network with eight nodes.

12
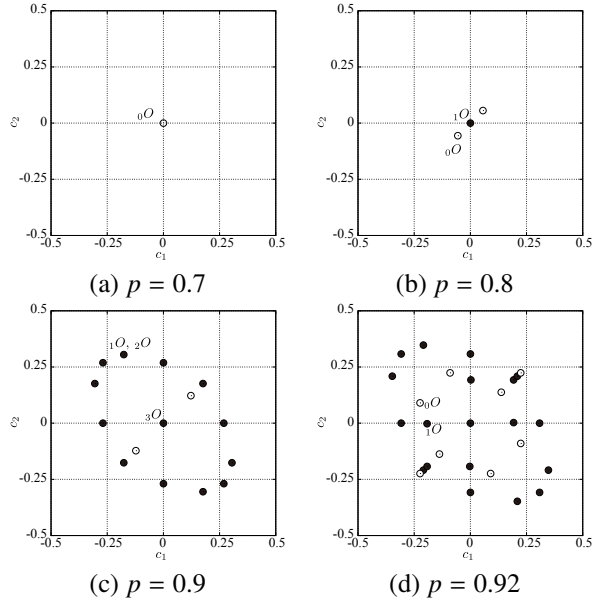
Figure 5: Equilibrium points for $\xi = -0.1$ with various values of p. Open and filled circles represent stable and unstable equilibria, respectively.

Next, we evaluate the bifurcation structures with a view toward the MAX-CUT problem solver. Note that the spin state x of the DOPO is presented as Eq. (7).

In Fig. 3, there is the trivial equilibrium point at the origin in region (i). In region (ii) after the pitchfork bifurcation, the original equilibrium becomes unstable while two stable equilibria appear around the origin. They take non-zero c_j values; thus, the DOPO network specifies two different cuts of the MAX-CUT problem. Table 3 lists the coordinates of the equilibrium points and their cuts for the target network. In region (ii), two equilibria are suboptimal. In region (iii), the six stable equilibrium points listed below the dashed line in Table 3 appear via six saddle-node bifurcations. These are the globally optimal solutions, and they co-exist with the two suboptimal points above the dashed line. From Fig. 3, the globally optimal solution of the network with $\xi = -0.1$ can be obtained with $p > 0.9172$.

(a) $p = 1$, $m = 8$

(b) $p = 1.2$, $m = 14$

(c) $p = 1.3$, $m = 44$

(d) $p = 1.4$, $m = 110$

(e) $p = 1.6$, $m = 112$

(f) $p = 1.8$, $m = 256$
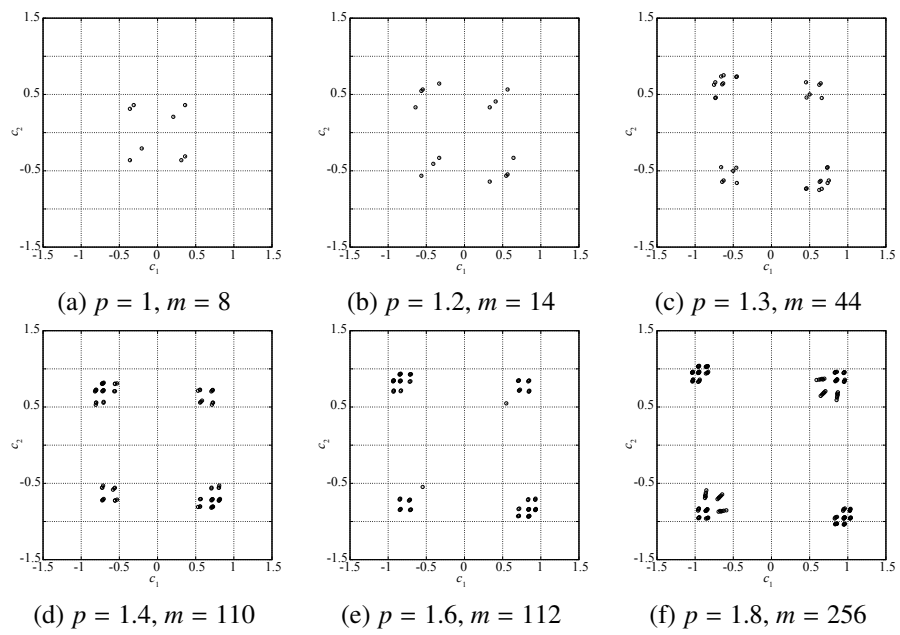
Figure 6: Locations of equilibrium points for $\xi = -0.1$. Here m indicates the number of stable equilibrium points.

14

Table 3: Stable equilibrium points of the DOPO network and their cut-size indices.

No.	$(c_1$	c_2	c_3	c_4	c_5	c_6	c_7	$c_8)$	Cut no.
				Region (i), i.e., $\xi = -0.1$, $p = 0.7$					
0	0	0	0	0	0	0	0	0	
				Region (ii), $\xi = -0.1$, $p = 0.8$					
1	+0.0560	+0.0560	+0.0560	−0.2258	−0.2258	−0.2258	+0.2554	+0.2554	xx
2	−0.0560	−0.0560	−0.0560	+0.2258	+0.2258	+0.2258	−0.2554	−0.2554	vii
				Region (iii), $\xi = -0.1$, $p = 0.92$					
1	+0.1377	+0.1377	+0.1377	−0.4117	−0.4117	−0.4117	+0.4447	+0.4447	xx
2	−0.1377	−0.1377	−0.1377	+0.4117	+0.4117	+0.4117	−0.4447	−0.4447	vii
3	+0.0903	−0.2240	−0.2240	+0.3683	+0.4251	+0.4251	−0.4422	−0.4422	iv
4	+0.2240	+0.2240	−0.0903	−0.4251	−0.4251	−0.3683	+0.4422	+0.4422	vi
5	+0.2240	−0.0903	+0.2240	−0.4251	−0.3683	−0.4251	+0.4422	+0.4422	v
6	−0.0903	+0.2240	+0.2240	−0.3683	−0.4251	−0.4251	+0.4422	+0.4422	iii
7	−0.2240	+0.0903	−0.2240	+0.4251	+0.3683	+0.4251	−0.4422	−0.4422	ii
8	−0.2240	−0.2240	+0.0903	+0.4251	+0.4251	+0.3683	−0.4422	−0.4422	i

The relaxation function values of equilibrium points in Eq. (9) are shown in Fig. 7. The solid and the dashed lines represent stable and unstable equilibrium points, respectively. The oscillation mode that minimizes the relaxation function corresponds to the ground state of the Ising Hamiltonian given by Eq. (6). Line (B) that indicates η of the equilibria no. 3–8 in Table 3 is smallest in $p > 0.9172$. This shows that $_0O$ is the ground state. Therefore, the choice of parameters affects the performance of the CIM.
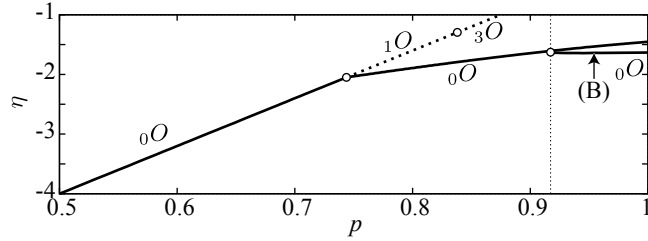
Figure 7: Relaxation function values of each stable equilibrium point in Eq. (9).

4. Bifurcation structure of network with different pump rates

In Section 3, we confirmed that the DOPO network model with common pump rates produces pitchfork bifurcations because it has particular symmetry. These bifurcations generate suboptimal solutions that co-exist with the globally optimal solution. Meanwhile, symmetric pitchfork and symmetry-breaking bifurcations are encountered widely in dynamical systems [28]. Golubitsky et al. used singularity theory to study imperfect bifurcations in a symmetrical model [26] and clarified the bifurcation structure with theoretical approach in the presence of imperfections [18, 29]. Mann et al. showed that a small parametric deviation from perfect symmetry replaces a pitchfork bifurcation with a saddle-node bifurcation [30]. Therefore, in the present case, if we were to adjust the parameters to remove the symmetry property, the resulting dynamics might inhibit the pitchfork bifurcations and so avoid suboptimal solutions.

In this section, we focus on the symmetry of the network and reveal the bifurcation structure when that symmetry is broken. Specifically, we investigate the bifurcation structure when some of the pump rates are varied to break symmetry on purpose, and discuss the potential of this approach for improving performance of the CIM. We as-

sume that m is the index number of nodes or DOPOs in the network (see Fig. 1) and that its pump rate is p_m. The mathematical model is re-described as follows:

$$\frac{d}{dt}c_j = \left(-1 + p_j - (c_j^2 + s_j^2)\right)c_j + \sum_{l=1,\,l \neq j}^{N} \xi_{jl}c_l,$$

$$\frac{d}{dt}s_j = \left(-1 - p_j - (c_j^2 + s_j^2)\right)s_j + \sum_{l=1,\,l \neq j}^{N} \xi_{jl}s_l,$$ (31)

$$\text{if} \quad j \neq m \qquad \text{then} \quad p_j = p,$$ (32)

for some $m \in (1, 2, \ldots, 8)$. We have modified the DOPO network model so that the pump rate p_m of the node with index number m is now an adjustable parameter as opposed to having a common parameter p for all nodes. Hence, the system loses the symmetry property δ_1 or δ_2 in Eq. (30). Note that we consider only $m = 1, 4$ and 7 herein because the other cases have entirely the same bifurcation structure because of the graph isomorphism corresponding to the network topology.

Figure 8 shows the bifurcation diagram in the p-p_1 plane. In particular, the diagonal line corresponds to line (A) in Fig. 3. The bifurcation curves split the whole region into subregions (iv)–(vii). In region (iv), all nodes converge to the origin. By a pitchfork bifurcation, two symmetrical stable equilibrium points are generated in region (v). When the pump rate increases further, six new equilibrium points emerge in region (vi) via saddle-node bifurcations. They co-exist with the two aforementioned equilibrium points. Their order of appearance corresponds to that found previously [8]. From Tables 2 and 3, note that the equilibrium points that emerge in regions (v) and (vi) are the suboptimal and globally optimal solutions, respectively.

Let us consider the case of nondiagonal parameter values, namely $p \neq p_1$. Figure 8(b) shows an enlarged region of Fig. 8 (a). The suboptimal solutions change to unstable equilibrium points in region (vii) via saddle-node or pitchfork bifurcations. This means that a CIM can always pick up the globally optimal solution for the target network in region (vii). Line (C) separating regions (v) and (vii) represents the parameter set for which the equilibrium point has a zero in-phase component, and c_j takes different signs on either side of this line. The stabilities of equilibria on both regions (v) and (vii) are the same because no bifurcations occur, so the solution found by the CIM

17

changes without any local bifurcations. Hence, the cut alters to the other cut which corresponds to the globally optimal solution without any bifurcation phenomenon for the network topology.
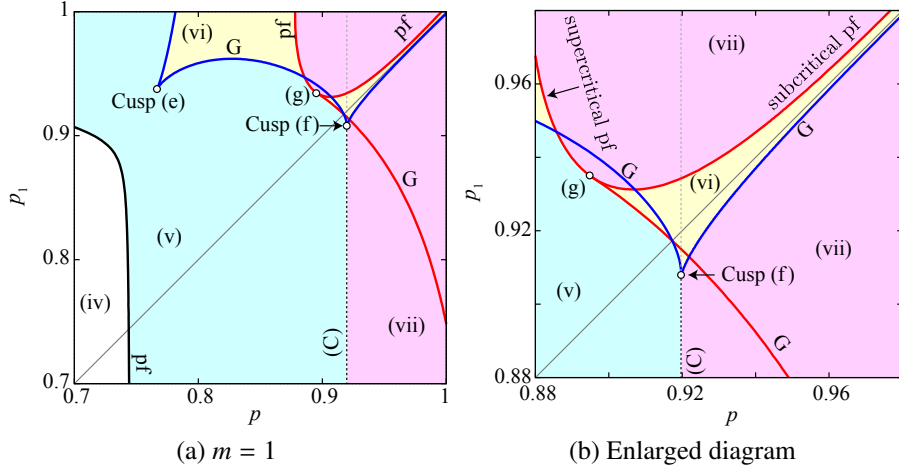
Figure 8: Bifurcation diagrams in the p-p_1 plane ($m = 1$). (b) shows an enlarged region of (a). Suboptimal solutions xx and vii exist in the regions (v) and (vi).

In Fig 8, some bifurcation parameter sets meet at the points (e), (f), and (g). In particular, a codimension-two bifurcation [22, 31, 32] is observed at points (e) and (f). To explain these structures, we employ an equilibrium manifold in $\mathbf{R}^3$. Figure 9 shows sketches of the bifurcation structure around (e) and (f), where the horizontal and vertical axes represent p and p_1, respectively.

Around cusp point (e), the manifold of the suboptimal solutions is independent of the cusp structure of the globally optimal solutions, and thus suboptimal solutions do not disappear around here. Hence, the suboptimal solutions co-exist with the globally optimal solutions. The manifold of the globally optimal solutions and unstable equilibrium points makes a cuspidal structure with two saddle-node bifurcations. Therefore, if the globally optimal solutions undergo a saddle-node bifurcation, it jumps catastrophically to a suboptimal solution [13, 33]. Around cusp point (f), the stable and unstable manifolds have the hysteretic structure shown in Fig. 9(b). There are three equilibrium points, namely the two stable ones and the unstable one between the two saddle-node bifurcations. If they undergo bifurcation, another catastrophic jump occurs.

(a) Cusp point (e)   (b) Cusp point (f)
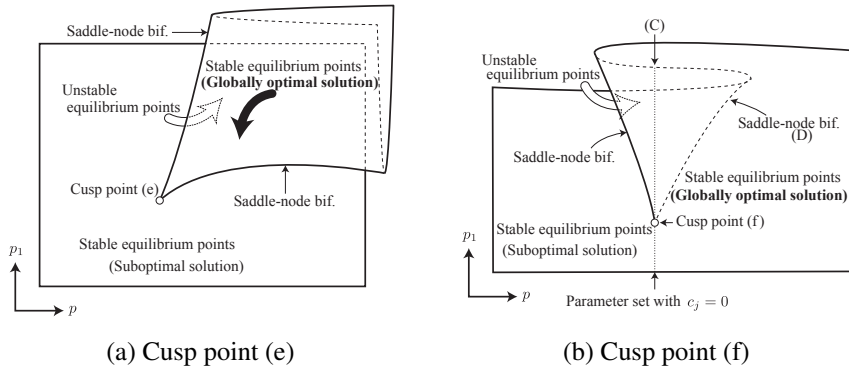
Figure 9: Equilibrium manifolds around cusp points (e) and (f). Three saddle-node bifurcation sets make two cusp structures. Two bifurcation curves intersect at the cusp point, thus a codimension-two bifurcation occurs.

Figure 10 illustrates the bifurcation structure and steady states around point (g). In the upper part of the figure, region (vii) is enclosed by a pair of bifurcation sets, each involving a supercritical and a subcritical pitchfork bifurcation. In this region, the suboptimal solutions become unstable and the globally optimal solutions appear through the supercritical pitchfork bifurcation. The saddle-node bifurcation that generates the globally optimal solutions approaches the pitchfork bifurcation curve at point (g). This is a singular point that connects the supercritical and subcritical pitchfork bifurcations. Consequently, the three bifurcation curves meet at point (g). Meanwhile, the suboptimal solution becomes an attractor via the subcritical pitchfork bifurcation again, but disappears via saddle-node bifurcation (D) in Fig. 9(b).
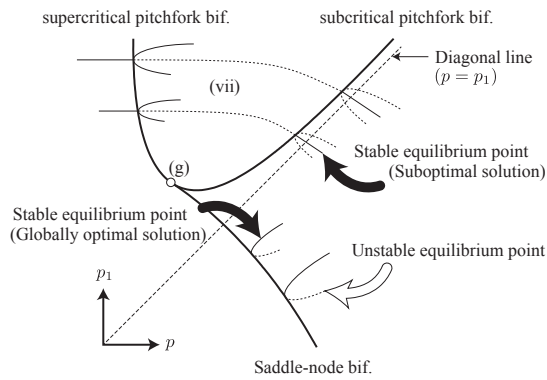
Figure 10: Steady-state structure around supercritical and subcritical pitchfork bifurcations.

19

Figure 11 shows the bifurcation diagrams for (a) $m = 4$ and (b) $m = 7$. For $m = 4$, region (vii) is smaller in the upper part of the diagram but broader in the lower part compared to the case for $m = 1$. Thus, we recommend configuring the pump rate as $p_4 < p$. By contrast, there is no region (vii) for $m = 7$, so the network cannot but be attracted to the suboptimal solutions. Note that in region (vi) a CIM could settle on either type of solution depending on the initial values because the globally optimal solutions co-exist with the suboptimal solutions.

(a) $m = 4$

(b) $m = 7$
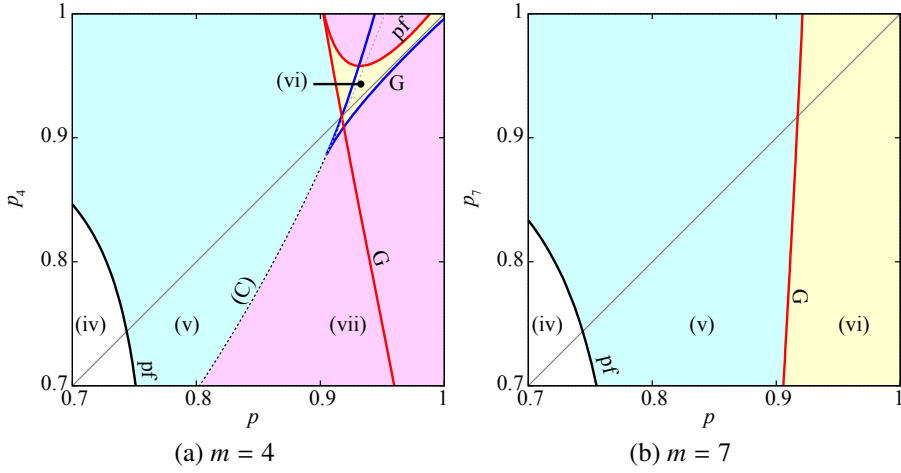
Figure 11: Bifurcation diagrams in the p-p_m plane. In the lower part of (a) for $m = 4$, region (vii) is broader than it is in Fig. 8. By contrast, there is no attraction region (vii) for $m = 7$ in the specified parameter range.

From these results, we have confirmed the bifurcation structures of the origin, the globally optimal and the suboptimal solutions in Fig. 8 for $m = 1$, 4, and 7. The shapes of regions (v) and (vi) depend on the index number m. In relation to improving CIM performance, the shapes provide important information for establishing a control strategy. If each node is pumped sufficiently, adjusting p_1 is an effective way to avoid suboptimal solutions. For $m = 4$, p_4 should be lower than the common pump rate p. However, the pump rate p_7 has no effect on CIM performance for $p < 1$ and $p_7 < 1$ because region (vii) does not exist. In summary, it is important to determine which nodes should be adjusted in which direction, and this requires a design scheme based on the topological characteristic of the network.

5. Conclusions

We have used numerical analysis to investigate bifurcation phenomena in a DOPO network intended as an Ising problem solver. We began by proving particular symmetry of a *P*-invariant DOPO model. If the network has a common pump rate, then the system has symmetry group $\Gamma = \{I_{2N}, -I_{2N}, \delta_j\}$. In particular, δ_j is a symmetric transformation involving an exchange of nodes the identify of which depends on the network topology. Next, we investigated the stability and bifurcations of the DOPO model in conjunction with explaining the numerical analysis process for detecting the equilibrium points and their bifurcations.

In the single model, the DOPO has only three equilibrium points, namely the origin and origin–symmetric-pair attractors. The origin undergoes just one pitchfork bifurcation at $p = 1$. The pair attractors that have positive and negative normalized in-phase components are generated through this bifurcation. They signify spin modes and remain as stable attractors for the pump rate $p > 1$.

Next, we analyzed eight coupled DOPOs numerically. In the network model, pitchfork and saddle-node bifurcations generate various attractors denoting spin configurations. In fact, for a sufficiently large pump rate, the model has $2^8 = 256$ equilibrium points that are all solutions of an eight-bit combinatorial problem. However, the ground state of the target network appears at $p = 0.9172$, so the CIM would require the pump rate to be set larger than an appropriate value so that the stable equilibrium point corresponding to the globally optimum solution exists. This value depends on the topology and the coupling matrix Ξ of the objective Ising problem. However, non-ground states also appear in a DOPO network in which the pump rate is common to all nodes, in some cases even before the emergence of the ground states. In the target network, they co-exist with the ground state at $p > 0.9127$. Hence, the CIM might locate a suboptimal solution, meaning that we cannot avoid suboptimal solutions by using a common pump rate. This circumstance reduces the probability of the CIM succeeding.

To find the parameter set for which the CIM locates only the ground state, we removed the assumption of a common pump rate. Specifically, we made the pump rate p_m of specific node *m* an adjustable parameter rather than have a common parameter *p* for

all nodes. By doing this, the symmetry properties disappear and symmetry-breaking bifurcations are observed. From the bifurcation diagram in the p-p_m plane, we confirmed that the non-ground states become unstable through pitchfork and saddle-node bifurcations. Hence, these results imply the existence of parameter sets for which the DOPO network always adopts the ground state. From the analysis results, we suggest that our strategy improves the probability of locating a globally optimal solution because adjusting the pump rate of an appropriate node can avoid local-optimal solutions. However, the efficacy of this strategy depends on which pumps are adjusted and how.

References

[1] A. Marandi, Z. Wang, K. Takata, R. L. Byer, Y. Yamamoto, Network of time-multiplexed optical parametric oscillators as a coherent Ising machine, Nat Photon 8 (12) (2014) 937–942.

[2] K. Takata, S. Utsunomiya, Y. Yamamoto, Transient time of an Ising machine based on injection-locked laser network, New Journal of Physics 14 (2012) 013052. doi:10.1088/1367-2630/14/1/013052.

[3] J. C. Gonzalez-Henao, E. Pugliese, S. Euzzor, S. F. Abdalah, R. Meucci, J. A. Roversi, Generation of entanglement in quantum parametric oscillators using phase control, Scientific Reports 5 (2015) 13152.

[4] F. Barahona, On the computational complexity of ising spin glass models, Journal of Physics A: Mathematical and General 15 (10) (1982) 3241.

[5] K. Takata, A. Marandi, R. Hamerly, Y. Haribara, D. Maruo, S. Tamate, H. Sakaguchi, S. Utsunomiya, Y. Yamamoto, A 16-bit Coherent Ising Machine for One-Dimensional Ring and Cubic Graph Problems, Scientific Reports 6 (2016) 34089.

[6] T. Inagaki, Y. Haribara, K. Igarashi, T. Sonobe, S. Tamate, T. Honjo, A. Marandi, P. L. McMahon, T. Umeki, K. Enbutsu, O. Tadanaga, H. Takenouchi, K. Aihara, K.-i. Kawarabayashi, K. Inoue, S. Utsunomiya, H. Takesue, A coherent Ising machine for 2000-node optimization problems, Science 354 (6312) (2016) 603–606. doi:10.1126/science.aah4243.

[7] P. L. McMahon, A. Marandi, Y. Haribara, R. Hamerly, C. Langrock, S. Tamate, T. Inagaki, H. Takesue, S. Utsunomiya, K. Aihara, R. L. Byer, M. M. Fejer, H. Mabuchi, Y. Yamamoto, A fully programmable 100-spin coherent Ising machine with all-to-all connections, Science 354 (6312) (2016) 614–617. doi:10.1126/science.aah5178.

[8] Z. Wang, A. Marandi, K. Wen, R. L. Byer, Y. Yamamoto, Coherent Ising machine based on degenerate optical parametric oscillators, Physical Review A 88 (6) (2013) 063853 (9 pages). doi:10.1103/PhysRevA.88.063853.

[9] Z. Wang, Coherent Computation in Degenerate Optical Parametric Oscillators, Ph.D. thesis, Stanford University, Stanford University, Stanford, CA 94305 USA (2015).

[10] R. M. Karp, Reducibility among Combinatorial Problems, in: Complexity of Computer Computations, Springer US, Boston, MA, 1972, pp. 85–103.

[11] M. X. Goemans, D. P. Williamson, Improved Approximation Algorithms for Maximum Cut and Satisfiability Problems Using Semidefinite Programming, Journal of the ACM 42 (6) (1995) 1115–1145. doi:10.1145/227683.227684.

[12] Y. Haribara, S. Utsunomiya, Y. Yamamoto, A coherent ising machine for MAX-CUT problems: Performance evaluation against semidefinite programming and simulated annealing, in: Principles and Methods of Quantum Information Technologies, Vol. 911 of Lecture Notes in Physics, Springer, Japan, 2016, Ch. 12, pp. 251–262.

[13] Y. Kuznetsov, Two-parameter bifurcations of equilibria in continuous-time dynamical systems, in: Elements of Applied Bifurcation Theory, Vol. 112 of Ap-

plied Mathematical Sciences, Springer-Verlag New York, 2004, Ch. 8, pp. 295–405.

[14] T. Shoji, K. Aihara, Y. Yamamoto, Quantum model for coherent ising machines: Stochastic differential equations with replicator dynamics, Phys. Rev. A 96 (5) (2017) 053833. doi:10.1103/PhysRevA.96.053833.

[15] A. Yamamura, K. Aihara, Y. Yamamoto, Quantum model for coherent ising machines: Discrete-time measurement feedback formulation, Phys. Rev. A 96 (5) (2017) 053834. doi:10.1103/PhysRevA.96.053834.

[16] S. Utsunomiya, K. Takata, Y. Yamamoto, Mapping of Ising models onto injection-locked laser systems, Optics Express 19 (19) (2011) 18091–18108. doi:10.1364/OE.19.018091.

[17] A. Galluccio, M. Loebl, J. Vondrák, New Algorithm for the Ising Problem: Partition Function for Finite Lattice Graphs, Physical Review Letter 84 (26) (2000) 5924–5927. doi:10.1103/PhysRevLett.84.5924.

[18] M. Golubitsky, D. Schaeffer, A theory for imperfect bifurcation via singularity theory, Communications on Pure and Applied Mathematics 32 (1) (1979) 21–98. doi:10.1002/cpa.3160320103.

[19] M. Golubitsky, I. Stewart, david schaeffer, Singularities and Groups in Bifurcation Theory, Vol. 69 of Applied Mathematical Sciences, Springer-Verlag New York, New York, NY, 1988. doi:10.1007/978-1-4612-4574-2.

[20] T. Ueta, H. Miyazaki, T. Kousaka, H. Kawakami, Bifurcation and Chaos in Coupled Bvp Oscillators, International Journal of Bifurcation and Chaos 14 (04) (2004) 1305–1324.

[21] H. Kitajima, Y. Katsuta, H. Kawakami, Bifurcations of Periodic Solutions in a Coupled Oscillator with Voltage Ports, IEICE transactions on fundamentals of electronics, communications and computer sciences 81 (3) (1998) 476–482.

[22] H. Kawakami, T. Yoshinaga, Codimension Two Bifurcation and Its Computational Algorithm, in: J. Awrejcewicz (Ed.), Bifurcation and Chaos, Theory and Applications, Springer Series in Nonlinear Dynamics, Springer Berlin Heidelberg, 1995, Ch. 6, pp. 97–132.

[23] U. M. Ascher, R. M. M. Mattheij, R. D. Russell, Numerical Solution of Boundary Value Problems for Ordinary Differential Equations, Society for Industrial and Applied Mathematics, 1995. doi:10.1137/1.9781611971231.

[24] T. Ueta, G. Chen, T. Yoshinaga, H. Kawakami, A numerical algorithm for computing Neimark-Sacker bifurcation parameters, in: Proceedings of the 1999 IEEE International Symposium on Circuits and Systems, Vol. 5, 1999, pp. 503–506. doi:10.1109/ISCAS.1999.777619.

[25] T. Ueta, H. Kawakami, Numerical Approaches to Bifurcation Analysis, Vol. 11 of World Scientific Series on Nonlinear Science Series B, World Scientific Publishing Co Pte Ltd, 2002, Ch. 28, pp. 593–610.

[26] M. Golubitsky, D. Schaeffer, Imperfect bifurcation in the presence of symmetry, Communications in Mathematical Physics 67 (3) (1979) 205–232.

[27] M. Matsumoto, T. Nishimura, Mersenne twister: a 623-dimensionally equidistributed uniform pseudo-random number generator, ACM Transactions on Modeling and Computer Simulation 8 (1) (1998) 3–30. doi:10.1145/272991.272995.

[28] A. H. Nayfeh, B. Balachandran, Applied Nonlinear Dynamics: Analytical, Computational and Experimental Methods, Wiley, 1995.

[29] M. Golubitsky, D. Schaeffer, An analysis of imperfect bifurcation, Annals of the New York Academy of Sciences 316 (1) (1979) 127–133. doi:10.1111/j.1749-6632.1979.tb29464.x.

[30] B. P. Mann, M. A. Koplow, Symmetry breaking bifurcations of a parametrically excited pendulum, Nonlinear Dynamics 46 (4) (2006) 427–437. doi:10.1007/s11071-006-9033-0.

[31] J. Guckenheimer, P. Holmes, Nonlinear Oscillations, Dynamical Systems, and Bi-furcations of Vector Fields, Vol. 42 of Applied Mathematical Sciences, Springer New York, New York, NY, 1983. doi:10.1007/978-1-4612-1140-2.

[32] V. I. Arnold, Geometrical Methods in the Theory of Ordinary Differential Equations, Vol. 250 of Grundlehren der mathematischen Wissenschaften, Springer New York, New York, NY, 1988. doi:10.1007/978-1-4612-1037-5.

[33] J. Harlim, W. F. Langford, The Cusp-Hopf Bifurcation, International Journal of Bifurcation and Chaos 17 (08) (2007) 2547–2570. doi:10.1142/S0218127407018622.